科学通报 2018 年 第 63 卷 第 15 期: 1502 ~ 1514
论 文
《中国科学》杂志社
SCIENCE CHINA PRESS

兴安地块下泥盆统古地磁结果对其古地理位置的制约

张东海, 黄宝春*, 赵千, 张也

北京大学地球与空间科学学院, 造山带与地壳演化教育部重点实验室, 北京 100871

*联系人, E-mail: bchuang@pku.edu.cn

2018-02-04 收稿, 2018-04-07 修回, 2018-04-09 接受, 2018-05-18 网络版发表

国家重点基础研究发展计划(2013CB429802)和国家自然科学基金重大项目(41190071)资助

摘要 兴安地块对中亚造山带的晚古生代演化过程具有重要意义, 然而其古地理位置目前仍无可靠古地磁数据限制. 本文选取黑龙江省多宝山地区的一个下泥盆统泥鳅河组紫红色粉砂岩剖面开展了系统古地磁学研究, 11个采点均显示高低温双分量特征. 低温分量在地理坐标系下与现代地磁场接近, 应为近代获得的黏滞剩磁或热黏滞剩磁; 高温分量显示单一负极性特征, 在35.7%褶皱展开处获得最大集中, 经与同时代乌里雅斯太陆缘和中蒙古额尔古纳地块的古地磁数据进行对比, 认为其可能遭受了附近309~299 Ma(石炭-二叠纪负极性超时期间)的花岗岩浆侵入热事件改造而获得重磁化特征剩磁分量: D/I=28.6°/−33.2°, k=18.6, α_{95}=10.9°, 对应的古地磁极为λ_p/φ_p=17.3°S/97.1°E(dp/dm=7.0°/12.4°). 结合同时代周边地块的古地磁数据分析认为: 晚石炭世中蒙古-额尔古纳地块、乌里雅斯太陆缘和兴安地块纬度差异小于3°, 可能已形成统一陆块, 位于28°~30°N附近; 此时西伯利亚位于45°~50°N附近而华北和松辽-锡林浩特地块则位于赤道低纬度地区; 古亚洲洋此时仍未关闭, 主洋盆为贺根山洋而非索伦洋.

关键词 古亚洲洋, 兴安地块, 同褶皱重磁化, 下泥盆统泥鳅河组, 古地磁学

中亚造山带是夹持于西伯利亚、华北、塔里木和东欧板块之间的显生宙增生造山带[1]. 其中古亚洲洋的演化一般认为是从早古生代的多岛洋格局逐渐通过大洋俯冲、侧向拼贴等过程在晚古生代完成最终闭合, 但关于其最终闭合时间和位置却争议很大[2~5]. 古亚洲洋的闭合整体呈现从西往东逐渐呈剪刀式闭合的特点, 闭合时间东边最晚[6]. 关于东古亚洲洋的最终闭合, 徐备等人[7]认为是早古生代沿南北造山带先后完成闭合, 晚古生代的主导地质过程则已转变为区域伸展. 邵济安等人[8]也认为晚古生代华北板块与中亚诸板块之间为陆壳基底之上发育的陆表海和裂陷槽而非宽阔的大洋洋盆. 而Xiao等人[3]则识别出6套代表活动陆缘和增生楔的构造单元, 认为温都尔庙增生杂岩、白乃庙岛弧以及贺根山、宝力道增生杂岩分别代表了古亚洲洋早古生代和晚古生代的俯冲记录, 直至晚二叠世才完成最终闭合.

以前的古地磁研究认为晚二叠世华北-蒙古联合块体已经形成, 其与西伯利亚的拼合则是晚侏罗世至早白垩世沿蒙古-鄂霍茨克缝合带闭合[9~13]. 而对于晚二叠世之前东古亚洲洋的演化, 古地磁研究提供的限定仍很缺乏. Zhao等人[14]在内蒙古板块(相当于本文松辽-锡林浩特地块, 图1(a))获得了一个晚泥盆世的古地磁极, 认为此时已经与华北、蒙古无古纬度差异, 古亚洲洋已经闭合. Zhao等人[13]在内蒙古天山镇采石场获得的晚石炭世古地磁极指示松辽-锡林浩特地块(图1(a))当时位于南纬4.3°, 而同时期华北板块位于北纬12°[15]. 李朋武等人[16]则认为内蒙古中部(包括本文中的乌里雅斯太陆缘、松辽-锡林浩特和华北北缘, 图1(a))在晚石炭世-早二叠世

引用格式: 张东海, 黄宝春, 赵千, 等. 兴安地块下泥盆统古地磁结果对其古地理位置的制约. 科学通报, 2018, 63: 1502–1514
Zhang D H, Huang B C, Zhao Q, et al. Paleomagnetic results from Lower Devonian sandstones of the Niqiuhe Formation in the Duobaoshan area and its constraints on paleoposition of the Xing'an block (in Chinese). Chin Sci Bull, 2018, 63: 1502–1514, doi: 10.1360/N972018-00142

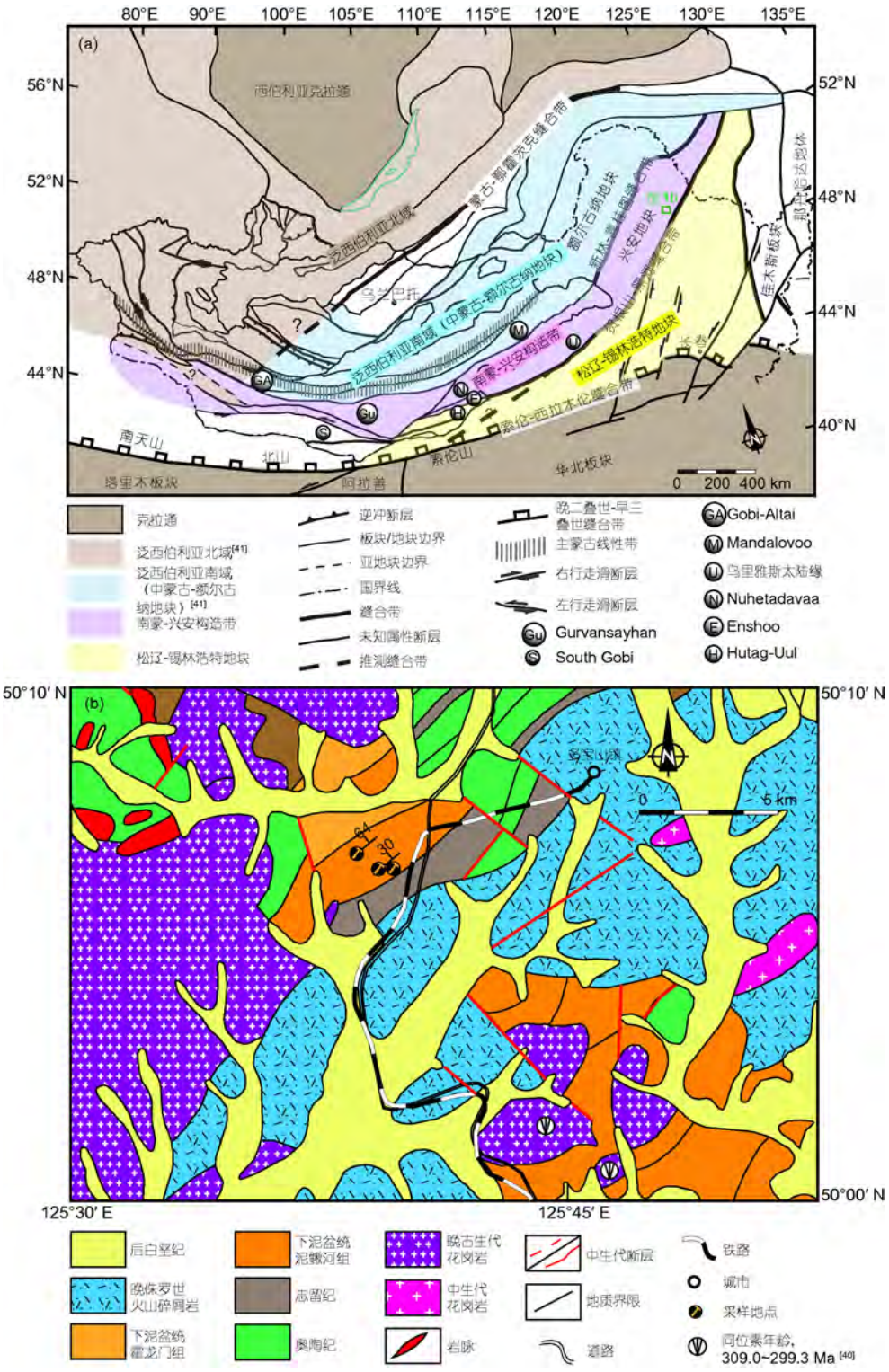

图 1 (网络版彩色)中亚造山带构造划分方案及研究区地质图. (a) 中亚造山带东段构造划分简图, 改自Badarch等人[17]、Kröner等人[18]、Cocks和Torsvik[19]及Liu等人[20]; (b) 采样地区地质图, 据1:200000地质图(卧都河幅)

Figure 1 (Color online) (a) Schematic tectonic division of the eastern Central Asian Orogenic Belt (CAOB), modified after Badarch et al.[17], Kröner et al.[18], Cocks and Torsvik[19] and Liu et al.[20]; (b) simplified geological map of the sampling area, according to the 1:200000 Woduhe geological map

位于17°~18°N, 与华北板块关系密切, 可能已经是华北板块的组成部分. 但Chen等人[21]在乌里雅斯太陆缘(图1(a))上石炭统宝力高庙组的结果则指示了~29°N的古纬度, 仍然与华北板块具有一定的间隔.

兴安地块被一些学者认为是乌里雅斯太陆缘的东延(图1(a))[7,20], 与额尔古纳地块在500 Ma已经沿新林-喜桂图缝合带闭合[20](图1(a)). 然而也有学者认为兴安地块应与蒙古Mandaloovo地体相连, 与乌里雅斯太陆缘不应视为同一陆块[22]. 贺根山-黑河缝合带是乌里雅斯太陆缘-兴安地块与松辽-锡林浩特地块的缝合带, 贺根山蛇绿岩的年龄约为310 Ma, 代表了此时贺根山洋已经闭合[20](图1(a)). 然而Miao等人[23]则认为贺根山蛇绿岩的侵位时间为~245 Ma, 在此期间古亚洲洋一直是南索伦洋北贺根山洋的两洋残留模式. 目前在兴安地块上仍无古生代古地磁数据发表, 笔者选取了贺根山-黑河缝合线北侧的多宝山地区下泥盆统泥鳅河组开展了系统古地磁学研究, 希望对早泥盆世兴安地块的古地理位置予以限定, 为其与东古亚洲洋其他微陆块的相对位置关系提供古地磁制约.

1 地质背景与古地磁采样

兴蒙造山带位于中亚造山带东段, 由北至南可分为额尔古纳地块、乌里雅斯太-兴安地块、松辽-锡林浩特地块、华北板块北缘, 并由新林-喜桂图缝合带、贺根山黑河缝合带及索伦-西拉木伦-长春-延吉缝合带分隔, 各地块均出露有前寒武纪基底(图1(a))[20]. 额尔古纳地块与兴安地块沿新林-喜桂图缝合带于~500 Ma闭合, 带内出露头道桥蓝片岩[24]及新林-吉峰蛇绿岩[25]. 乌里雅斯太-兴安地块与松辽-锡林浩特地块的拼合时间认识不一, 从早石炭世[20,26]至晚二叠世-早三叠世[2,22,23], 贺根山-黑河缝合带内出露贺根山蛇绿岩和嫩江蓝片岩. 松辽-锡林浩特地块与华北板块的拼合一般认为代表了东古亚洲洋的闭合, 徐备等人[7]认为其拼合于420 Ma之前已经完成, 也有观点[3,20,23,27]认为持续至晚二叠世至早三叠世, 甚至中晚三叠世[2].

研究区位于黑龙江省嫩江县多宝山镇西南(图1(b)), 区内地层由下到上出露奥陶系至第四系沉积岩、火山碎屑岩, 古生代地层广泛遭受海西期晚期及燕山期早期花岗岩浆作用改造, 普遍经历低级区域变质作用, 缺失下石炭统、下二叠统、中下侏罗统及上白垩统[28]. 其中下泥盆统泥鳅河组由下而上分为泥鳅河碎屑岩段、罕达气中酸性火山岩段及金水碎屑岩、安山岩段, 下伏上志留统卧都河组石英砂岩、粉砂岩, 上覆下泥盆统霍龙门组碎屑岩, 地层内含有丰富的海相化石, 包括腕足类(*Leptocoelia sinica*, *Gladio strophia kondoi*及*Acrospirifer dyadobomus*等组合)及珊瑚类化石[28]. 本次研究选取了位于通往采石场道路两侧泥鳅河组碎屑岩段的两个紫红色粉砂岩剖面进行了古地磁采样(图2), 平均每个采点10~14块样品, 共计11个采点112块样品. 所有样品在野外均采用磁罗盘定向, 条件允许时还另外采用了太阳罗盘定向. 研究区平均磁偏角为−12.4°, 所有数据均进行了磁偏角校正.

2 实验方法与结果

2.1 实验方法

在进行实验前所有古地磁定向样品均被加工成2.54 cm×2.2 cm的标准样品, 我们选取了部分切割后的

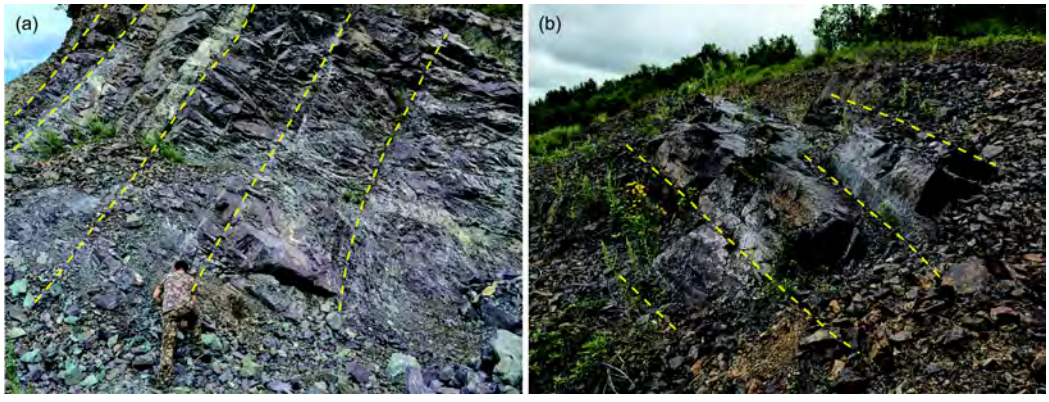

图 2 (网络版彩色)采样剖面照片. (a) 路北侧采石场内露头; (b) 路南侧露头; 二者具有倾角差异

Figure 2 (Color online) Representative photos of the sampling section showing. (a) The quarry outcrop located to the north of the road; (b) outcrop to the south of the road with distinct dip angles

碎样进行了系统岩石磁学实验，在中国科学院青藏高原研究所大陆碰撞与高原隆升重点实验室古地磁实验室使用AGICO MFK1卡帕桥进行磁化率温度变化曲线(κ-T)测试. 另外在中国科学院地质与地球物理研究所古地磁与年代学实验室(PGL)使用Micromag 3900 振荡样品磁强计进行了磁滞回线、等温剩磁(IRM)获得曲线及反向场退磁曲线测试. 所有样品均在北京大学构造磁学实验室进行了系统热退磁实验，通常样品先在ASC TD-48S热退磁炉内进行加热，到达目标温度后保持30~40 min再进行冷却，然后再使用2G-755-4K低温超导岩石磁力仪进行剩磁测量. 500℃以前通常采用50~100℃为间隔，500℃以后温度间隔逐渐减小(10~20℃)，部分样品在670℃以后采取2℃间隔进行退磁. 对大部分退磁结果使用了主成分分析法(PCA)进行分析[29]，确定剩磁方向一般使用了4个以上的温度点数据，并且平均角偏差(MAD)小于10°. 部分样品则采用重磁化大圆弧交会法进行统计[30]，统计出来的方向使用Fisher统计方法[31]进行了平均. 古地磁数据的处理主要采用PMGSC(Version 4.2)[32]和Pmagpy[33]等软件进行处理.

2.2 岩石磁学实验结果

两个代表样品(MN175-8和MN180-9)的磁化率温度变化曲线(κ-T)均呈现升温与降温曲线不可逆的特征，可能在加热过程中存在新生磁性矿物的生成. 两组κ-T曲线在约400~585℃区间均出现显著的磁化率增加，可能指示了Hopkinson效应，即单畴磁铁矿的存在(图3(a), (b))[34]. 600℃以后磁化率仍然存在显著的降低，表明了样品中赤铁矿的大量存在. 磁滞回线结果显示样品具有较大的矫顽力(Bc = 270~370 mT; 图4(a), (e)), IRM获得曲线及反向场退磁曲线结果指示样品的剩磁矫顽力(Bcr)为297~363 mT(图4(b), (f)), 指示了样品中具有高矫顽力组分的存在. 矫顽力谱分析[35](图4(c), (d), 4(g)~(h))指示样品的主要载磁矿物的矫顽力为316~398 mT, 同时还存在6%~8%的低矫顽力组分(~16 mT). 综合以上实验结果，可以看出样品的主要载磁矿物为赤铁矿和少量磁铁矿.

2.3 退磁结果

112块样品中有5块样品未能获得有效退磁数据，其余样品均显示为高低温双分量特征(图5)，其中低温分量大部分于400~500℃完全退去(图5(a), (c), (e), (g)), 该分量与现代地磁场方向十分接近(图6)，可能为黏滞剩磁或新生代以来获得的热黏滞剩磁. 在低温分量被分离后，高温特征剩磁分量通常在500~680℃之间稳定地趋向于原点，反映了特征分量的载磁矿物主要为赤铁矿，该分量在产状校正前后均显示为单一负极性(图5, 7(a), (b)). 随后我们对每个采点的高温分量进行采点内Fisher平均，得到每个采点的平均剩磁方向，然后再将其进行Fisher平均得到采点平均特征剩磁方向. 泥鳅河组紫红色粉砂岩11个采点的采点平均方向在产状校正前为D/I=16.6°/−36.1°, k=17.3, α_{95}=11.3°, 产状校正后为D/I=42.7°/−20.4°, k=15.5, α_{95}=12.0° (表1, 图7(a), (b)). 尽管采样地层为单斜地层，但分布于道路两侧采

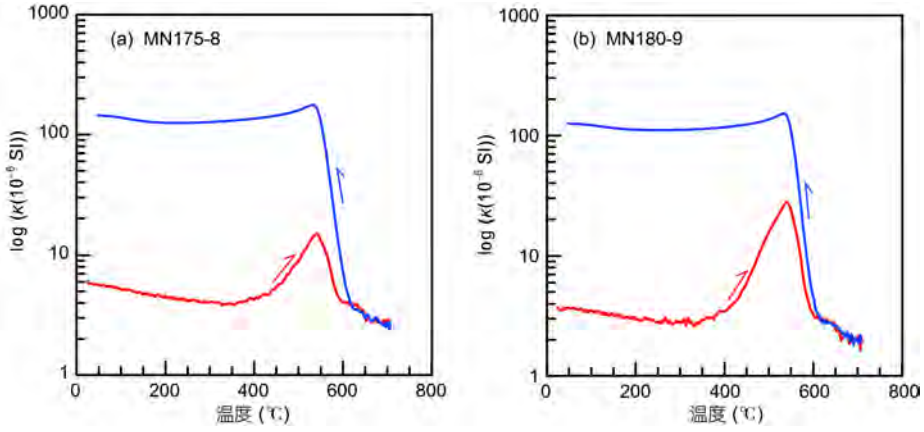

图 3 采样剖面代表性样品磁化率温度曲线图. 其中红色为升温曲线, 蓝色为降温曲线

Figure 3 Magnetic susceptibility variation of temperature (κ-T) curves of representative samples. Red (blue) lines represent the heating (cooling) processes

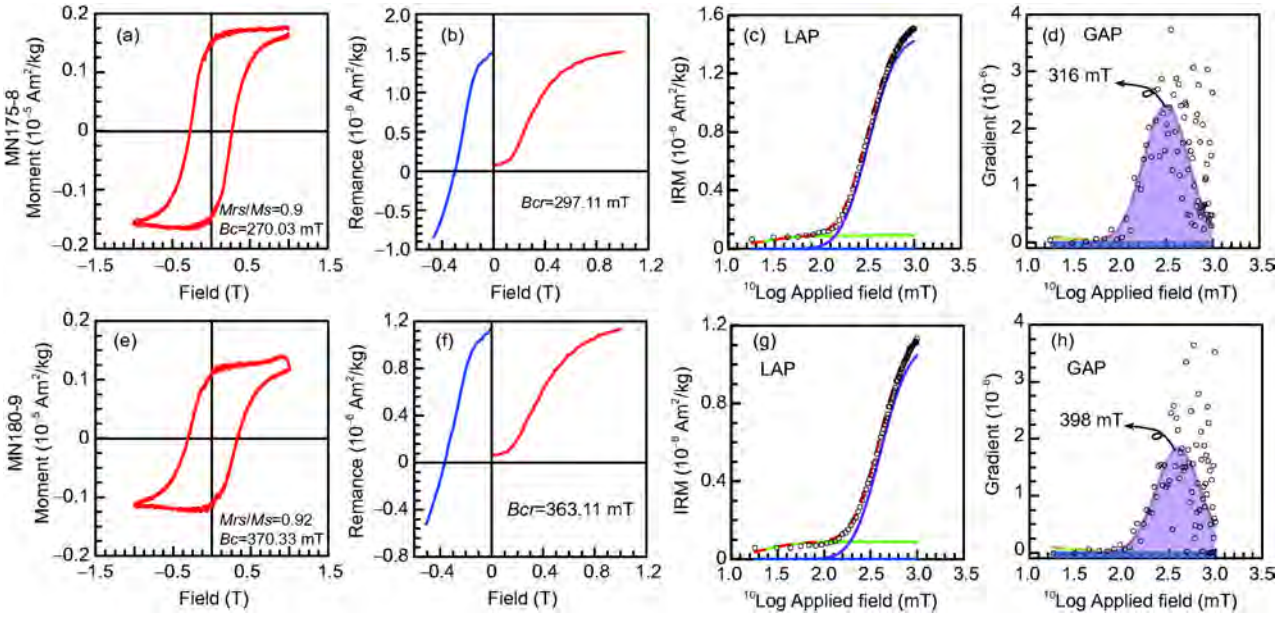

图 4 采样剖面代表性样品的(a, e)磁滞回线, (b, f)等温剩磁获得曲线(红色)和反向场退磁曲线(蓝色); 矫顽力谱分析的(c, g)线性获得曲线投图和(d, h)梯度获得曲线投图(Kruvier等人[35])

Figure 4 Representative rock magnetic results of the sampling section. (a, e) Hysteresis loops; (b, f) Acquisition curves of isothermal remnant magnetization (IRM) (red lines) and back-field demagnetization curves (blue lines); (c, g) linear acquisition plot (LAP) and (d, h) gradient acquisition plot (GAP) of the coercivity spectra analysis (Kruiver et al.[35])

样剖面地层仍然显示出了一定的倾角变化(约30°~60°, 表1). 应用McFadden[37]的褶皱检验显示在褶皱前后的ξ_2值分别为2.388和6.5, 并于36%展开处获得最大集中, 指示95%置信区间下的负褶皱检验(临界值ξ=3.865).

进一步应用Watson和 Enkin[38]逐步展开褶皱检验显示剩磁方向在 (35.7±11.7)%处获得最大集中(表1, 图7(c), (d)), 反映特征剩磁分量应为同褶皱构造作用过程中获得. 采样剖面35.7%展开处的平均特征剩磁分量方向为D/I=28.6°/−33.2°(k=18.6, α_{95}=10.9°), 对应的古地磁极为λ_p/φ_p=17.3°S/97.1°E(dp/dm=7.0°/12.4°)(表1, 图7(c)).

3 讨论

3.1 剩磁获得时间

内蒙古-黑龙江大兴安岭地区泥盆纪-中二叠世主要显示为NW-SE向的构造应力场, 而晚二叠世至早三叠世则转换为近S-N向[39], 这表明研究区在晚二叠世发生了构造应力转换. 研究区奥陶系至泥盆系主要呈NE-SW走向(图1(b)), 表明其褶皱作用所受应力应主要为NW-SE向. 另外, 区内可见泥盆系与上二叠统星火组的角度不整合[28](图1(b)). 以上两点表明奥陶系至泥盆系的地层主要受晚二叠世以前的NW-SE向应力作用发生了褶皱作用, 褶皱时间为中泥盆世至中二叠世, 并于晚二叠世再次接受星火组沉积. 采样剖面的特征剩磁分量显示于35.7%褶皱展平处获得最大集中, 指示剩磁应该是在褶皱作用中晚期获得, 可能为晚石炭世至中二叠世期间. 另外, 曲晖等人[40]对研究区附近的晚古生代碱长花岗岩和正长花岗岩的SHRIMP测年结果分别为309.0±3.0 Ma和299.3±2.8 Ma. 采样剖面距离最近的一个晚古生代花岗侵入岩体不足3 km(图1(b)), 采样地层及更老的奥陶系-志留系地层均被切穿, 这首先表明采样地层的时代应老于钉合岩体的侵入年龄, 来自古生物的证据对泥鳅河组成岩时代为早泥盆世[28]的限定应是可靠的; 其次指示了采样剖面很可能是由于此次花岗岩浆侵入热事件而获得的重磁化. 另外, 11个采点的特征剩磁分量在地理/地层坐标系下均显示单一负极性, 这对于沉积岩并不常见, 因为沉积岩的成岩过程相较于火山岩经历了更长的时间跨度, 除非其成岩时代为石炭纪-二叠纪负极性超时期间(约318~262 Ma)[41], 否则很难不记录正极性期的地球磁场, 而上述来自钉合岩体[40]和古生物[28]的证据均表明采样地层形成于早泥盆世, 所以该特征剩磁分量应为在石炭纪-二叠纪负

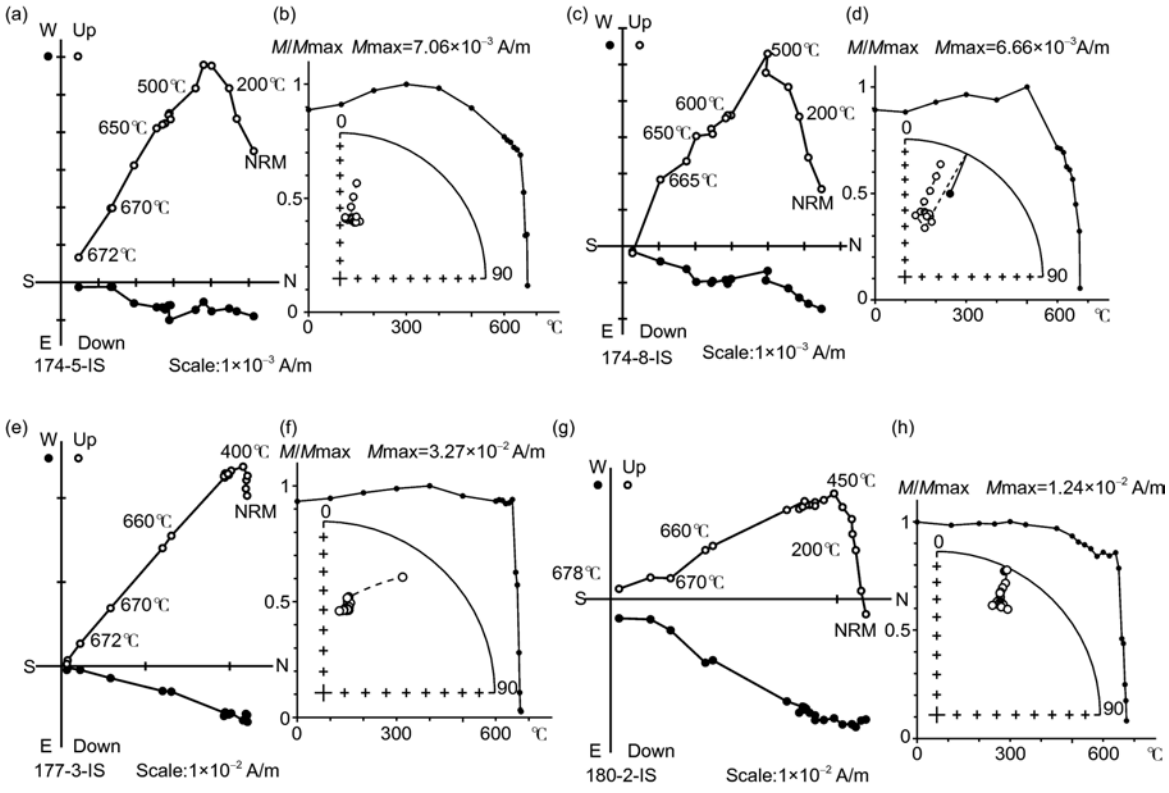

图 5 泥鳅河组代表性样品的热退磁结果. (a, c, e, g) 地理坐标系下正交矢量投影, 实心(空心)圆圈代表水平(垂直)投影; (b, d, f, h) 强度衰减曲线和等面积投影图

Figure 5 (a, c, e, g) Representative orthogonal (Zijderveld) vector plots of the sampling section in geographic coordinates; solid (open) circles represent horizontal (vertical) projection. (b, d, f, h) Magnetization variation dependence of temperature and equal area plots of the stepwise demagnetization

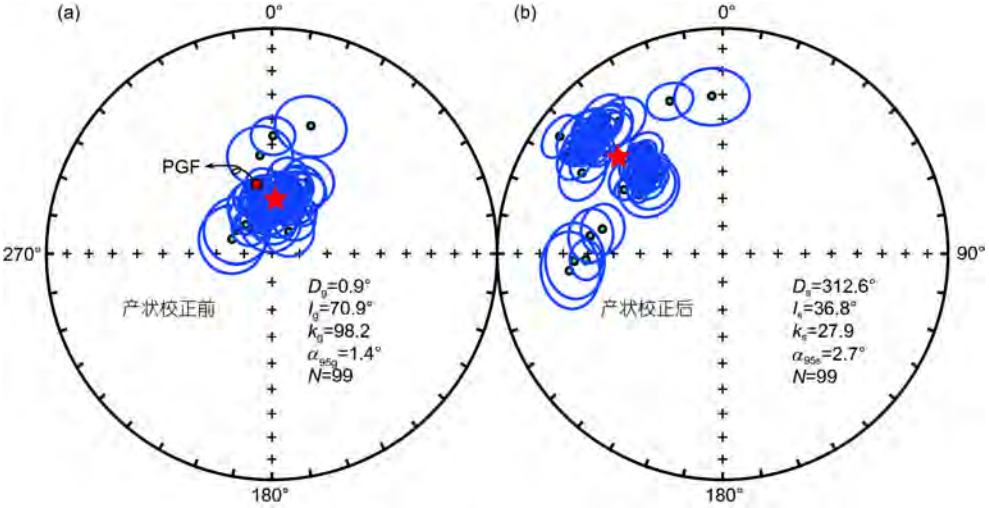

图 6 采样剖面低温分量在(a)地理坐标系和(b)地层坐标系下的等面积投影图. PGF: 现代地磁场方向; 红色五角星代表低温分量的Fisher平均方向, 实心(空心)圆代表下半球(上半球)投影

Figure 6 Equal area plots of the low temperature component (a) before and (b) after tilt correction. PGF: Present geomagnetic field; red stars are mean directions of the low temperature components. Solid (open) circles represent lower (upper) hemisphere projections

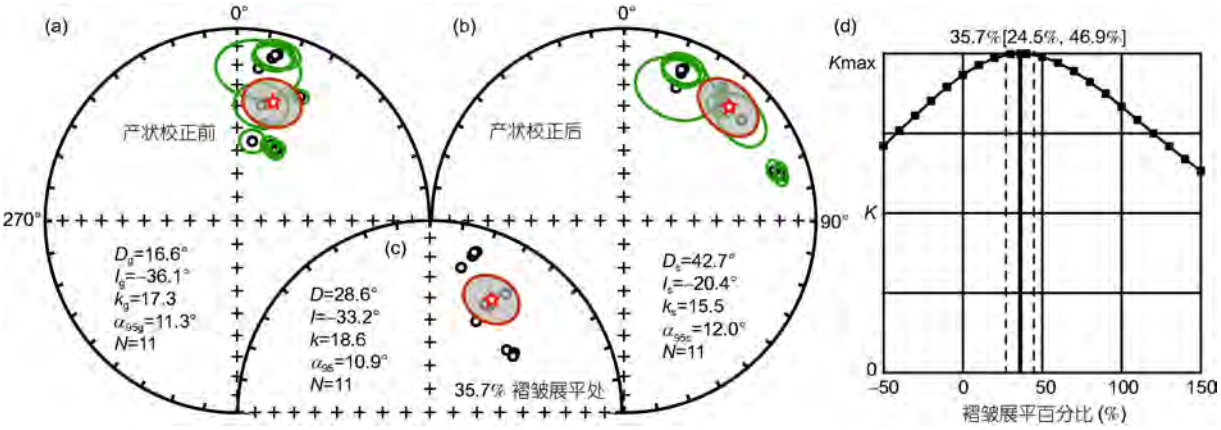

图 7 采样剖面采点平均特征剩磁分量的等面积投影图. (a) 产状校正前; (b) 产状校正后; (c) 35.7%褶皱展开处; (d) 逐步展开褶皱检验结果[38]. 其他同图6

Figure 7 Equal area plots of the site-mean ChRM directions of the sampling section. (a) Before, (b) after and (c) at 35.7% unfolding. (d) Stepwise unfolding analysis[38]. The rest is the same as for Figure 6

表 1 兴安地块下泥盆统泥鳅河组砂岩采样信息及特征剩磁分量采点平均数据[a)]

Table 1 Summary of sampling information and characteristic remanence (ChRMs) from Lower Devonian Niqiuhe Formation sandstones in the Xing'an Block (XB), NE China

采点号	λ_s (°N)	φ_s (°E)	走向/倾角(°)	n	R/N	D_g (°)	I_g (°)	D_s (°)	I_s (°)	κ	α_{95} (°)	φ_p (°E)	λ_p (°N)
MN173	50.1007	125.6486	196/61	9	9/0	11.9	–38.4	49.4	–20.5	25.0	10.5	114.1	–17.5
MN174	50.1007	125.6486	199/64	10	10/0	23.3	–54.7	71.6	–18.6	180.9	3.6	106.8	–2.2
MN175	50.1007	125.6486	199/64	11	11/0	29.0	–54.6	72.7	–15.5	217.8	3.1	102.3	–1.0
MN176	50.1007	125.6486	199/64	7	7/0	28.7	–56.1	74.1	–16.2	316.0	3.4	103.0	0.4
MN177	50.0978	125.6441	163/45	9	9/0	15.6	–46.9	36.6	–14.9	1838.8	1.2	111.7	–10.6
MN178	50.0978	125.6441	163/45	10	10/0	10.7	–55.4	39.7	–23.3	94.3	5.0	117.0	–3.4
MN179	50.0980	125.6440	205/30	14	14/0	12.2	–14.5	21.2	–18.8	37.2	6.6	111.4	–31.6
MN180	50.0980	125.6440	205/30	8	8/0	26.9	–28.4	41.6	–23.3	300.4	3.2	97.8	–20.6
MN181	50.0980	125.6440	205/30	10	10/0	13.7	–12.0	21.5	–16.0	41.4	7.6	109.4	–32.6
MN182	50.0980	125.6440	205/30	10	10/0	12.9	–12.6	20.8	–17.0	51.4	6.8	110.4	–32.4
MN183	50.0980	125.6440	205/30	9	9/0	7.9	–21.0	21.4	–26.6	12.9	14.9	116.8	–28.6
采点平均方向				11	11/0	16.6	–36.1			17.3	11.3		
				11				42.7	–20.4	15.5	12.0		
采点平均方向 (35.7%褶皱展平处)				11		28.6	–33.2			18.59	10.9		
平均虚地磁极 (35.7%褶皱展平处)				11						dp=7.0	dm=12.4	97.1	–17.3

a) λ_s/φ_s (λ_p/φ_p): 采样点(地理坐标系下的方向对应的虚地磁极)纬度/经度; n: 参与统计的样品/采点数量; R/N: 显示负/正极性的样品数或采点数; D_g/I_g (D_s/I_s): 地理坐标系(层面坐标系)下的偏角/倾角; κ &α_{95}: 平均方向的精度参数和95% 置信区间; dp/dm: 平均虚地磁极95%置信椭圆的半长轴和半短轴. (1) McElhinny[36]褶皱检验: k_s/k_g=0.90<F(20, 20)=2.12, 指示95%置信区间内褶皱检验结果不确定; (2) McFadden[37]褶皱检验; 褶皱前后的ξ_2值分别为2.388和6.5, 指示95%置信区间内的负褶皱检验(临界值ξ=3.865), 在36%展开处获得重磁化; (3) Watson和Enkin[38]褶皱检验: (35.7±11.7)%处获得最大集中

极性超时期间的这次花岗岩浆侵入热事件中获得. 综上所述, 我们认为采样剖面的特征剩磁分量应为晚石炭世(309~299 Ma)获得的重磁化分量.

3.2 晚石炭世兴安地块的古地理位置

一般认为兴安地块与额尔古纳地块的拼合应于

~500 Ma时已沿新林-喜桂图缝合带完成，缝合带内出露的头道桥蓝片岩[24]及新林蛇绿岩[42]、吉峰-嘎县超基性岩[25]均支持这一论断. 而乌里雅斯太陆缘是否与兴安地块为同一地块仍存争议. Eizenhöfer和Zhao[22]将兴安地块与Mandalovoo地块相连，而乌里雅斯太陆缘则划为贺根山弧后盆地与Enshoo地体相连(图1(a)). 而Liu等人[20]则将兴安地块与乌里雅斯太陆缘统一归为兴安地块，Cocks和Torsvik[19]也类似地将二者统一视为Nuhetadavaa地体(图1(a))，他们提出泛西伯利亚构造域的边界应位于Gobi-Altai-Mandalovoo地体与Gurvan-sayhan地体之间，在此边界以南的地体与北部的中蒙古-额尔古纳等块体的拼贴可能于晚古生代晚期才完成(图1(a)). 因此，来自南蒙古-兴安构造带内的Gurvan-sayhan、乌里雅斯太陆缘及兴安地块晚石炭世是否与北部的中蒙古-额尔古纳地块为统一块体仍不清楚，但这几个陆块晚石炭世相似的古生物分布[43]表明它们相距不会太远.

相对于同一参考点(43°N, 114°E), 我们本次于多宝山地区下泥盆统泥鳅河组中获得的晚石炭世重磁化分量指示了兴安地块的古纬度为27.7°±12.4°N，Chen等人[21]于乌里雅斯太镇上石炭统宝力高庙组凝灰岩和安山岩中获得的古纬度数据则指示此时乌里雅斯太陆缘位于28.5°±9.7°N，此时兴安地块与乌里雅斯太陆缘此时的纬度差异为0.8°±9.9°，表明二者很可能已成为统一地块. 而来自中蒙古-额尔古纳地块赤塔附近的上石炭统岩石结果却指示了19.9°±14.8°N的古纬度[12]，相比乌里雅斯太-兴安地块似乎存在约7.8°~8.6°的纬度差. 与Chen等人[21]不同, 该结果是从砂岩中获得, 碎屑岩中

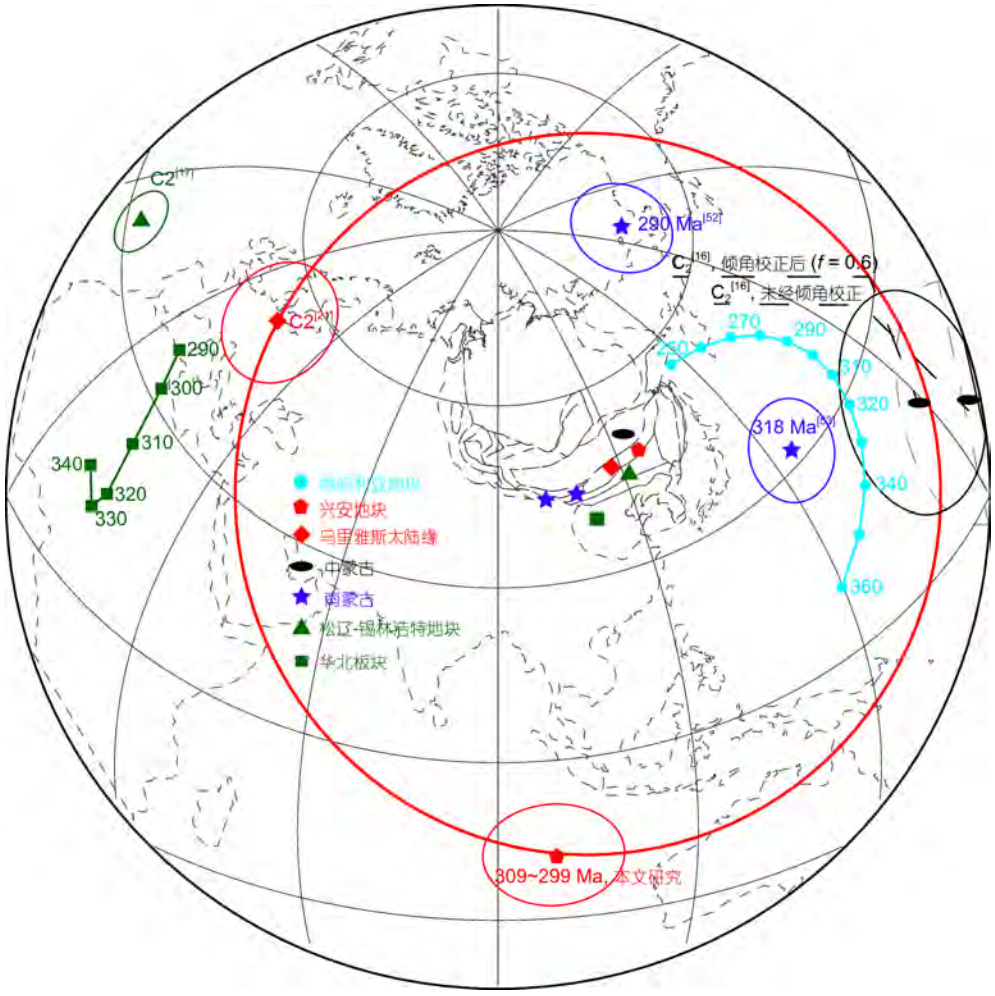

图 8 (网络版彩色)晚石炭世-早二叠世中亚造山带东段块体的古地磁极的施密特投影图. 小圆弧圆心为参考点(43°N, 114°E). 数据来自表2

Figure 8 (Color online) Schmidt projections of Late Carboniferous to Early Permian paleomagnetic poles from the eastern CAOB (Table 2). The small circle is centered on a reference site at 43°N/114°E

表 2 中亚造山带东段块体石炭纪至早二叠世古地磁数据[a)]

Table 2 Summary of Late Paleozoic to Mesozoic paleomagnetic data from the eastern CAOB

时代 (Ma)	平均年龄 (Ma)	岩性	采样地点	采点纬度(°N)	采点经度(°E)	*S*[*N*]	极纬度(°)	极经度(°)	期望值(参考点: 43°N, 114°E) $A_{95}(dp/dm)$	*D*(°)	*I*(°)	α_{95}(°)	古纬度(°)	△λ(°)	C.	参考文献
华北板块视极移曲线																
290	290	–	–	–	–	–	37.3	6.5	–	308.6	26.1	–	13.8	–	–	Huang等人[51]
300	300	–	–	–	–	–	32.1	10.4	–	302.5	23.9	–	12.5	–	–	Huang等人[51]
310	310	–	–	–	–	–	23.6	13.8	–	294.1	17.4	–	8.9	–	–	Huang等人[51]
320	320	–	–	–	–	–	15.4	15.4	–	287.1	8.6	–	4.3	–	–	Huang等人[51]
330	330	–	–	–	–	–	12.1	14.2	–	285.5	2.4	–	1.2	–	–	Huang等人[51]
340	340	–	–	–	–	–	15.8	10.0	–	291.0	1.8	–	0.9	–	–	Huang等人[51]
松辽-锡林浩特地块																
$P_{1\text{-}3}$	265	C, V	内蒙古林西	43.7	118.4	6	48.7	3.7	6.9	318.7	22.8	7.8	20.2	6.9	F	Zhao等人[14]
C_2-P_1	300	L	内蒙古天山镇	43.9	120.1	4[29]	32.6	338.1	4.4	324.0	−8.6	6.1	−4.3	4.4	F	Zhao等人[13]
南蒙-兴安地块																
乌里雅斯太陆缘																
C_2	320	V	内蒙古东乌旗	45.5	117.2	5	53.4	14.8	9.7	317.9	47.4	9.3	28.5	9.7	–	Chen等人[21]
兴安地块																
C_2 (309~299)	305	C	黑龙江多宝山	50.1	125.6	11	−17.3	97.1	7.0/12.4	198.3	46.4	9.0	27.7	12.4	IS	本文研究
南蒙古																
290	290	G	Hanbogd	–	–	–	71.0	188.0	7.8	26.4	63.7	5.5	45.3	7.8	BC	Kovalenko[52]
318	318	V	Noen-Tost	43.1	101.0	[42]	32.2	154.6	7.8	95.0	71.6	4.7	56.4	7.8	F	Kovalenko 和Chernov[53]
333	333	V	–	45.0	96.0	22	–	–	–	–	53.2	4.7	33.8	7.0	F	Bazhenov[48]
C_1	340	C	Nomgon	–	–	–	−10.0	150.0	4.9	139.2	46.4	4.8	27.7	4.9	F	Kovalenko[52]
*C_1	340	–	–	–	–	–	0.2	143.0	4.9	140.8	59.2	3.8	39.9	4.9	–	–
中蒙古-额尔古纳地块																
C_2 (320~296)	308	C	Chiron	51.53	115.4	8	10.2	186.2	14.8	94.6	35.9	16.7	19.9	14.8	F	Xu等人[16]
*C_2 (320~296)	308	–	–	–	–	–	18.8	179.0	14.8	92.5	50.0	13.5	30.8	14.8	–	–
C_1 (363~333)	348	C	Zeya	53.6	127	8	39.8	31.6	10.0/15.5	297.6	49.9	16.9	30.7	10.0	F	Kravchinsky等人[54]
*C_1 (363~333)	348	–	–	–	–	–	49.1	46.0	10.0/15.5	302.4	62.6	9.0	44.0	10.0	–	–
西伯利亚视极移曲线																
250	250	–	–	–	–	–	56.1	146.2	–	46.2	77.3	–	65.7	–	–	Torsvik等人[47]
260	260	–	–	–	–	–	54.2	156.2	–	52.9	74.2	–	60.5	–	–	Torsvik等人[47]
270	270	–	–	–	–	–	51.1	163.7	–	58.6	71.3	–	55.9	–	–	Torsvik等人[47]
280	280	–	–	–	–	–	47.1	168.6	–	64.3	68.7	–	52.0	–	–	Torsvik等人[47]
290	290	–	–	–	–	–	42.8	171.2	–	69.9	66.5	–	48.9	–	–	Torsvik等人[47]
300	300	–	–	–	–	–	38.2	172.1	–	75.8	64.6	–	46.5	–	–	Torsvik等人[47]
310	310	–	–	–	–	–	34.0	171.4	–	81.5	63.5	–	45.1	–	–	Torsvik等人[47]
320	320	–	–	–	–	–	29.4	169.2	–	88.4	62.9	–	44.3	–	–	Torsvik等人[47]
330	330	–	–	–	–	–	24.7	166.0	–	96.0	62.6	–	44.0	–	–	Torsvik等人[47]
340	340	–	–	–	–	–	20.1	161.6	–	104.6	62.8	–	44.2	–	–	Torsvik等人[47]
350	350	–	–	–	–	–	15.6	156.1	–	114.2	63.4	–	44.9	–	–	Torsvik等人[47]
360	360	–	–	–	–	–	11.1	149.4	–	125.4	64.0	–	45.7	–	–	Torsvik等人[47]

a) *S*[*N*]: 用于计算平均古地磁极的采点数[样品数]; L: 用于平均的采样地点数; A_{95} (α_{95}): 古地磁极(期望方向)的95% 置信区间; *D*, *I*: 换算到同一参考点下的期望偏角、倾角; △λ: 古纬度误差; C: 碎屑岩; L: 灰岩; V: 火山岩; G: 花岗岩; C.: 评论; F: 褶皱检验; IS: 地理坐标系; BC: 烘烤检验; *代表使用倾角浅化因子f=0.6 进行校正后的数据. 在本文所选取的年龄范围内, 华北板块和西伯利亚板块的视极移曲线都是通过火山岩、侵入岩或者灰岩中获得的古地磁数据建立的, 一般认为无倾角浅化问题[15,47]

的剩磁倾角浅化问题近些年来已经被广泛讨论[44,45], 而国际上的全球重建研究中对于这些数据的处理通常是使用统一的倾角浅化因子f=0.6进行校正[11,46,47]. 在利用此方法对赤塔的数据进行倾角浅化校正后, 指示了30.8°±14.8°N的古纬度, 与乌里雅斯太陆缘和兴安地块的纬度差异(3.2°±12.8°)在古地磁置信范围不显著, 表明兴安地块、乌里雅斯太陆缘与中蒙古-额尔古纳地块此时很可能已成为统一陆块, 位于大约28°~30°N附近. 来自3个地块的古地磁极虽然不能重合, 但沿参考点为圆心的小圆弧分布(图8), 其差异可能是由中生代显著的走滑断层作用所导致的局部旋转引起的[14,48,49].

此时的西伯利亚位于约45°~50°N附近(表2), 表明与南部的中蒙古-额尔古纳地块和乌里雅斯太-兴安地块处于不同的古纬度, 这可能是由于晚泥盆世蒙古鄂霍茨克洋的张开所致[22]. 另一方面, 此时的华北板块和松辽-锡林浩特地块则位于赤道附近地区(表2): 华北板块位于4.3°~12.5°N, Zhao等人[13]在内蒙古阿鲁科尔沁旗天山镇灰岩的结果也指示了松辽-锡林浩特地块具有较低的古纬度(4.3°±4.4°S). 古生物方面, 晚石炭世至早二叠世的腕足动物群研究表明分隔北部冷水型动物为代表的北极大区与南部暖水型动物为代表的特提斯大区的分界线并非西拉木伦河一线, 而是在佳蒙地块中部通过[50], 他们这里定义的佳蒙地块为位于蒙古-鄂霍茨克带、西拉木伦河-延吉缝合带、中锡霍特俯冲带所围限的晚古生代统一地块. 在Wang等人[43]的重建模型中, 他们认为佳蒙地块横跨北极大区与特提斯大区的分界线(~45°N), 因此南北缘表现为不同的腕足动物群分布, 分隔佳蒙地块与华北板块的大洋仍被其放置在西拉木伦-延吉缝合带一线. 而从本文的研究看来, 这一分界线很可能为北部分隔乌里雅斯太-兴安地块与南部松辽-锡林浩特地块的贺根山黑河缝合带, 此时东古亚洲洋的主洋盆应为贺根山洋, 而南部的索伦洋则可能为一狭窄的残留洋盆. 近来多项研究表明, 贺根山蛇绿岩的形成于石炭纪, 而仰冲侵位时间不早于270 Ma[22,23], 也表明了贺根山洋的消亡应该不早于晚二叠世.

4 结论

通过对黑龙江省多宝山地区下泥盆统泥鳅河组紫红色粉砂岩剖面的古地磁研究, 从11个采点中获得了一个晚石炭世(309~299 Ma)的重磁化特征剩磁分量: D/I = 28.6°/−33.2°, k = 18.6, α_{95} = 10.9°, 对应的古地磁极为λ_p/φ_p = 17.3°S/97.1°E(dp/dm=7.0°/12.4°). 结合来自中蒙古-额尔古纳地块、乌里雅斯太陆缘、松辽锡林浩特地块和华北板块的数据认为, 此时中蒙古-额尔古纳地块、乌里雅斯太陆缘和兴安地块已无纬度差异, 可能已形成统一陆块, 位于28°~30°N附近, 而此时西伯利亚则位于更北靠近45°~50°N的位置, 华北和松辽-锡林浩特地块则位于赤道低纬度地区, 古亚洲洋此时仍未关闭, 主洋盆为贺根山洋而非索伦洋.

致谢 感谢两位匿名审稿人对本文提出的宝贵修改意见. 司机王伟在野外采样过程中提供的大力帮助. 感谢北京大学Thomas Berndt博士对英文摘要提供的润色修改.

参考文献

1 Şengör A M C, Natal'in B A, Burtman V S. Evolution of the Altaid tectonic collage and Palaeozoic crustal growth in Eurasia. Nature, 1993, 364: 299–307
2 Xiao W, Windley B F, Han C, et al. Late Paleozoic to early Triassic multiple roll-back and oroclinal bending of the Mongolia collage in Central Asia. Earth-Sci Rev, 2018, http://dx.doi.org/10.1016/j.earscirev.2017.09.020
3 Xiao W, Windley B F, Hao J, et al. Accretion leading to collision and the Permian Solonker suture, Inner Mongolia, China: Termination of the central Asian orogenic belt. Tectonics, 2003, 22: 1–20
4 Xu B, Charvet J, Chen Y, et al. Middle Paleozoic convergent orogenic belts in western Inner Mongolia (China): Framework, kinematics, geochronology and implications for tectonic evolution of the Central Asian Orogenic Belt. Gondwana Res, 2013, 23: 1342–1364
5 Xu B, Zhao P, Wang Y, et al. The pre-Devonian tectonic framework of Xing'an–Mongolia orogenic belt (XMOB) in north China. J Asian Earth Sci, 2015, 97: 183–196
6 Li J Y. Permian geodynamic setting of Northeast China and adjacent regions: Closure of the Paleo-Asian Ocean and subduction of the Paleo-Pacific Plate. J Asian Earth Sci, 2006, 26: 207–224
7 Xu B, Zhao P, Bao Q Z, et al. Preliminary study on the pre-Mesozoic tectonic unit division of the Xing-Meng Orogenic Belt (XMOB) (in Chinese).

Acta Petrol Sin, 2014, 30: 1841–1857 [徐备, 赵盼, 鲍庆中, 等. 兴蒙造山带前中生代构造单元划分初探. 岩石学报, 2014, 30: 1841–1857]
8 Shao J A, Tang K D, He G Q. Early Permian tectono-palaeogeographic reconstruction of Inner Mongolia, China (in Chinese). Acta Petrol Sin, 2014, 30: 1858–1866 [邵济安, 唐克东, 何国琦. 内蒙古早二叠世构造古地理的再造. 岩石学报, 2014, 30: 1858–1866]
9 Pruner P. Palaeomagnetism and palaeogeography of Mongolia from the Carboniferous to the Cretaceous—Final report. Phys Earth Planet Inter, 1992, 70: 169–177
10 Ren Q, Zhang S, Wu H, et al. Further paleomagnetic results from the ~155 Ma Tiaojishan Formation, Yanshan Belt, North China, and their implications for the tectonic evolution of the Mongol–Okhotsk suture. Gondwana Res, 2016, 35: 180–191
11 Van der Voo R, van Hinsbergen D J, Domeier M, et al. Latest Jurassic–earliest Cretaceous closure of the Mongol-Okhotsk Ocean: A paleomagnetic and seismological-tomographic analysis. Geol Soc Am Spec Pap, 2015, 513: 589–606
12 Xu X, Harbert W, Dril S, et al. New paleomagnetic data from the Mongol–Okhotsk collision zone, Chita region, south-central Russia: Implications for Paleozoic paleogeography of the Mongol–Okhotsk ocean. Tectonophysics, 1997, 269: 113–129
13 Zhao D, Horiuchi S, Hasegawa A. 3-D seismic velocity structure of the crust and the uppermost mantle in the northeastern Japan Arc. Tectonophysics, 1990, 181: 135–149
14 Zhao P, Chen Y, Xu B, et al. Did the Paleo-Asian Ocean between North China Block and Mongolia Block exist during the late Paleozoic? First paleomagnetic evidence from central-eastern Inner Mongolia, China. J Geophys Res Solid Earth, 2013, 118: 1873–1894
15 Wu H N, Zhu R X, Liu C, et al. Paleomagnetic observations in North China block: From Late Paleozoic to Triassic (in Chinese). Chin J Geophys, 1990, 33: 694–701 [吴汉宁, 朱日祥, 刘椿, 等. 华北地块晚古生代至三叠纪古地磁研究新结果及其构造意义. 地球物理学报, 1990, 33: 694–701]
16 Li P, Zhang S, Gao R, et al. New Upper Carboniferous–Lower Permian paleomagnetic results from the central Inner Mongolia and their geological implications (in Chinese). J Jilin Univer Earth Sci Ed, 2012, 1: 423–434 [李朋武, 张世红, 高锐, 等. 内蒙古中部晚石炭世—早二叠世古地磁新数据及其地质意义. 吉林大学学报(地球科学版), 2012, 1: 423–434]
17 Badarch G, Dickson Cunningham W, Windley B F. A new terrane subdivision for Mongolia: Implications for the Phanerozoic crustal growth of Central Asia. J Asian Earth Sci, 2002, 21: 87–110
18 Kröner A, Lehmann J, Schulmann K, et al. Lithostratigraphic and geochronological constraints on the evolution of the Central Asian Orogenic Belt in SW Mongolia: Early Paleozoic rifting followed by late Paleozoic accretion. Am J Sci, 2010, 310: 523–574
19 Cocks L R M, Torsvik T H. The dynamic evolution of the Palaeozoic geography of eastern Asia. Earth-Sci Rev, 2013, 117: 40–79
20 Liu Y, Li W, Feng Z, et al. A review of the Paleozoic tectonics in the eastern part of Central Asian Orogenic Belt. Gondwana Res, 2017, 43: 123–148
21 Chen H, Dobson J P, Heller F, et al. Preliminary paleomagnetic results from the Upper Carboniferous of Uliastai Block, Inner Mongolia, China. Geophys Res Lett, 1997, 24: 2833–2836
22 Eizenhöfer P R, Zhao G. Solonker Suture in East Asia and its bearing on the final closure of the eastern segment of the Palaeo-Asian Ocean. Earth-Sci Rev, 2018, http://dx.doi.org/10.1016/j.earscirev.2017.09.010
23 Miao L, Fan W, Liu D, et al. Geochronology and geochemistry of the Hegenshan ophiolitic complex: Implications for late-stage tectonic evolution of the Inner Mongolia-Daxinganling Orogenic Belt, China. J Asian Earth Sci, 2008, 32: 348–370
24 Zhou J B, Wang B, Wilde S A, et al. Geochemistry and U–Pb zircon dating of the Toudaoqiao blueschists in the Great Xing'an Range, northeast China, and tectonic implications. J Asian Earth Sci, 2015, 97: 197–210
25 Feng Z, Liu Y, Liu B, et al. Timing and nature of the Xinlin–Xiguitu Ocean: Constraints from ophiolitic gabbros in the northern Great Xing'an Range, eastern Central Asian Orogenic Belt. Int J Earth Sci (Geol Rundsch), 2015, 105: 491–505
26 Feng Z, Jia J, Liu Y, et al. Geochronology and geochemistry of the Carboniferous magmatism in the northern Great Xing'an Range, NE China: Constraints on the timing of amalgamation of Xing'an and Songnen blocks. J Asian Earth Sci, 2015, 113: 411–426
27 Song S, Wang M M, Xu X, et al. Ophiolites in the Xing'an-Inner Mongolia accretionary belt of the CAOB: Implications for two cycles of seafloor spreading and accretionary orogenic events. Tectonics, 2015, 34: 2221–2248
28 Heilongjiang Geological and Mineral Bureau. Regional Geology of Heilongjiang Province (in Chinese). Beijing: Geological Publishing House, 1993 [黑龙江省地质矿产局. 黑龙江省区域地质志. 北京: 地质出版社, 1993]
29 Kirschvink J L. The least-squares line and plane and the analysis of palaeomagnetic data. Geophys J Int, 1980, 62: 699–718
30 McFadden P L, McElhinny M W. The combined analysis of remagnetization circles and direct observations in palaeomagnetism. Earth Planet Sci Lett, 1988, 87: 161–172
31 Fisher R. Dispersion on a Sphere. Proc R Soc A-Math Phys Eng Sci, 1953, 217: 295–305
32 Enkin R, Wuolle K, Mccann C, et al. PMGSC–Paleomagnetism Data Analysis, User's Guide ver. 4.2. Geological Survey of Canada, 2003
33 Tauxe L, Shaar R, Jonestrask L, et al. PmagPy: Software package for paleomagnetic data analysis and a bridge to the Magnetics Information Consortium (MagIC) Database. Geochem Geophys Geosyst, 2016, 17: 2450–2463

34 Radhakrishnamurty C, Likhite S D. Hopkinson effect, blocking temperature and Curie point in basalts. Earth Planet Sci Lett, 1970, 7: 389–396

35 Kruiver P P, Dekkers M J, Heslop D. Quantification of magnetic coercivity components by the analysis of acquisition curves of isothermal remanent magnetisation. Earth Planet Sci Lett, 2001, 189: 269–276

36 McElhinny M. Statistical significance of the fold test in palaeomagnetism. Geophys J Int, 1964, 8: 338–340

37 McFadden P L. A new fold test for palaeomagnetic studies. Geophys J Int, 1990, 103: 163–169

38 Watson G S, Enkin R J. The fold test in paleomagnetism as a parameter estimation problem. Geophys Res Lett, 1993, 20: 2135–2137

39 Liu B. Study on the late Paleozoic tectonic evolution of the Great Xing'an Ranges (in Chinese). Doctor Dissertation. Changchun: Jilin University, 2014 [刘兵. 大兴安岭地区晚古生代构造演化研究. 博士学位论文. 长春: 吉林大学, 2014]

40 Qu H, Li C L, Zhao Z H, et al. Zircon U–Pb ages and geochemical characteristics of the granites in Duobaoshan area, Northeast Da Hinggan Mountains (in Chinese). Geol China, 2011, 38: 292–300 [曲晖, 李成禄, 赵忠海, 等. 大兴安岭东北部多宝山地区花岗岩锆石U-Pb年龄及岩石地球化学特征. 中国地质, 2011, 38: 292–300]

41 Irving E, Pullaiah G. Reversals of the geomagnetic field, magnetostratigraphy, and relative magnitude of paleosecular variation in the phanerozoic. Earth-Sci Rev, 1976, 12: 35–64

42 Li R. Xinlin Ophiolite (in Chinese). Heilongjiang Geol, 1991, 2: 19–32 [李瑞山. 新林蛇绿岩. 黑龙江地质, 1991, 2: 19–32]

43 Wang C, Zhao G, Li N, et al. Coevolution of brachiopod paleobiogeography and tectonopaleogeography during the late Paleozoic in Central Asia. Sci China Earth Sci, 2013, 56: 2084–2106

44 Kodama K P. Simplification of the anisotropy-based inclination correction technique for magnetite- and haematite-bearing rocks: A case study for the Carboniferous Glenshaw and Mauch Chunk Formations, North America. Geophys J Int, 2009, 176: 467–477

45 Tauxe L, Kodama K P, Kent D V. Testing corrections for paleomagnetic inclination error in sedimentary rocks: A comparative approach. Phys Earth Planet Inter, 2004, 145: 101–116

46 Torsvik T H, Müller R D, Van der Voo R, et al. Global plate motion frames: Toward a unified model. Rev Geophys, 2008, 46: 1–44

47 Torsvik T H, Van der Voo R, Preeden U, et al. Phanerozoic polar wander, palaeogeography and dynamics. Earth-Sci Rev, 2012, 114: 325–368

48 Bazhenov M L, Kozlovsky A M, Yarmolyuk V V, et al. Late Paleozoic paleomagnetism of South Mongolia: Exploring relationships between Siberia, Mongolia and North China. Gondwana Res, 2016, 40: 124–141

49 Zhao P, Faure M, Chen Y, et al. A new Triassic shortening-extrusion tectonic model for Central-Eastern Asia: Structural, geochronological and paleomagnetic investigations in the Xilamulun Fault (North China). Earth Planet Sci Lett, 2015, 426: 46–57

50 Wang C W, Sun Y W, Li N, et al. Tectonic implications of Late Paleozoic stratigraphic distribution in Northeast China and adjacent region. Sci China Ser D-Earth Sci, 2009, 52: 619–626 [王成文, 孙跃武, 李宁, 等. 中国东北及邻区晚古生代地层分布规律的大地构造意义. 中国科学D辑: 地球科学, 2009, 52: 1429–1437

51 Huang B, Yan Y, Piper J D A, et al. Paleomagnetic constraints on the paleogeography of the East Asian blocks during Late Paleozoic and Early Mesozoic times. Earth-Sci Rev, 2018, https://doi.org/10.1016/j.earscirev.2018.02.004

52 Kovalenko D V. Paleomagnetism of Late Paleozoic, Mesozoic, and Cenozoic rocks in Mongolia. Rus Geol Geophys, 2010, 51: 387–403

53 Kovalenko D V, Chernov E E. Paleomagnetism of Carboniferous-Permian and early jurassic geological complexes in Mongolia. Izv Phys Solid Earth, 2008, 44: 427–441

54 Kravchinsky V A, Sorokin A A, Courtillot V. Paleomagnetism of Paleozoic and Mesozoic sediments from the southern margin of Mongol-Okhotsk ocean, far eastern Russia. J Geophys Res, 2002, 107: EPM 10-1–EPM 10-22

Summary for “兴安地块下泥盆统古地磁结果对其古地理位置的制约”

Paleomagnetic results from Lower Devonian sandstones of the Niqiuhe Formation in the Duobaoshan area and its constraints on paleoposition of the Xing’an block

Donghai Zhang, Baochun Huang*, Qian Zhao & Ye Zhang

Key Laboratory of Orogenic Belt and Crust Evolution, Ministry of Education, School of Earth and Space Sciences, Peking University, Beijing 100871, China
*Corresponding author, E-mail: bchuang@pku.edu.cn

Two common but contradictory views toward the timing of the final closure of the eastern Paleo-Asian Ocean (PAO) are either the Pre-Late Devonian or the Late Permian to Early Triassic. Previous paleomagnetic studies support a consolidation of the unified North China and Mongolia by the Late Permian. However, Pre-Late Permian paleogeography of the eastern Central Asian Orogenic Belt (CAOB) is not well understood due to the scarcity of reliable paleomagnetic records. The Xing’an block plays a key role in the evolution of the CAOB, however, no paleomagnetic results are available so far to provide constraints on its Late Paleozoic paleo-position. We performed a systematic paleomagnetic study on a purple siltstone section of the Lower Devonian Niqiuhe Formation near the Duobaoshan County, Heilongjiang Province. Representative fresh end samples were subjected to rock magnetic analysis to identify their dominant magnetic carriers and particle size distribution. Rock magnetic experiments include measurements of magnetic susceptibility variation dependence of temperature (κ-T) curves, hysteresis loops, acquisition of isothermal remanent magnetization (IRM) and back-field demagnetization of saturated IRM (SIRM) curves. The results indicate that the magnetic remanence carriers are dominant by hematite with minor contributions of magnetite. 112 cylindrical specimens were thermally demagnetized using an ASC TD-48S furnace and measured in a 2G-755-4K SQUID system in the Magnetotectonics Lab of Peking University. A total of 11 sites revealed identical bi-components character. The low temperature component resembles the present geomagnetic field in geographic coordinates, while the high temperature characteristic remanence (ChRM) component was reversed polarity both before and after tilt correction. Optimal concentration is achieved at 35.7% unfolding percentage, which suggests the magnetization was acquired during the late stage of a folding process. A previous structural study indicated that stress field of the research area switched from NW-SE to N-S orientation during the Late Permian, which is supported by the predominant NE-SW oriented Ordovician to Devonian strata as well as the angular unconformity between the Devonian and Upper Permian strata. The folding time of the Niqiuhe Formation is likely Middle Devonian to Middle Permian. Supported by evidence from a suite of granites near our sampling section (less than 3 km) dating at 309−299 Ma along with the universal reversed polarity of all 11 sites, we argue that the ChRM component was acquired during the Permo-Carboniferous Reversed Superchron (~318−262 Ma), when the study area was affected by a granitic intrusion thermal event (309−299 Ma). The ChRM component (D/I=28.6°/−33.2°, k=18.6, α_{95}=10.9°) corresponds to a paleomagnetic pole of λ_p/φ_p=17.3°S/97.1°E (dp/dm=7.0°/12.4°). For a common reference site (43°N/114°E), our results suggest the Xing’an block was situated at 27.7°±12.4°N during the Late Carboniferous. Coeval results obtained from rocks of different lithology suggest 28.5°±9.7°N and 19.9°±14.8°N for the Uliastai continental margin and the Central Mongolia-Euruna block. After applying a blanket flattening factor f=0.6 for results obtained from clastic sedimentary rocks, the paleolatitudinal difference between the Xing’an block, Uliastai continental margin, and the Central Mongolia-Erguna block is less than 3.2°±12.8°. Late Carboniferous paleomagnetic poles from those three blocks are distributed along a small circle. Significant post-Permian local rotations are likely attributed to extensive Mesozoic strike-slip faults among the eastern CAOB. Those three blocks were probably consolidated into a unified block, situated at ~28°−30°N during the Late Carboniferous and dominant by the cold water Borel realm fauna. By contrast, the North China and Songliao-Xilinhot blocks was situated at an equatorial region (4.3°S−12°N) and dominant by the warm water Tethyan realm fauna, while Siberia was located at ~45°−50°N. The Paleo-Asian Ocean therefore remained open and the main basin was the Hegenshan ocean rather than the Solonker ocean.

Paleo-Asian Ocean, Xing’an block, synfolding remagnetization, lower devonian Niqiuhe formation, paleomagnetism

doi: 10.1360/N972018-00142